AD-A149 989 AN ORTHOGONAL GRID TECHNIQUE FOR STUDYING INTERNAL DEFORMATION AND ENERGY..(U) ARMY BALLISTIC RESEARCH LAB ABERDEEN PROVING GROUND MD W J BRUCHEY ET AL. DEC 84 1/1

UNCLASSIFIED BRL-MR-3415 SBI-AD-F300 549 F/G 19/4 NL

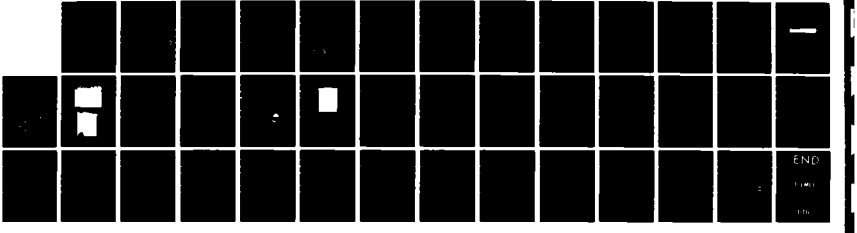

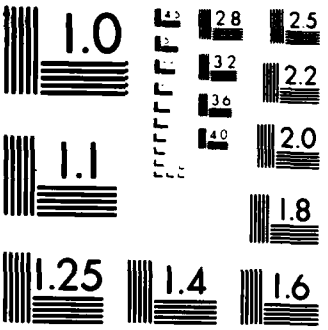

(12)

AD-A149 989

AD

BRL

MEMORANDUM REPORT BRL-MR-3415

AN ORTHOGONAL GRID TECHNIQUE FOR STUDYING INTERNAL DEFORMATION AND ENERGY ABSORPTION IN TARGET PENETRATION

William J. Bruchey
Jeffery T. Glass

December 1984

US ARMY BALLISTIC RESEARCH LABORATORY
ABERDEEN PROVING GROUND, MARYLAND

Destroy this report when it is no longer needed.
Do not return it to the originator.

Additional copies of this report may be obtained from the National Technical Information Service, U. S. Department of Commerce, Springfield, Virginia 22161.

The findings in this report are not to be construed as an official Department of the Army position, unless so designated by other authorized documents.

The use of trade names or manufacturers' names in this report does not constitute indorsement of any commercial product.

UNCLASSIFIED

SECURITY CLASSIFICATION OF THIS PAGE *(When Data Entered)*

REPORT DOCUMENTATION PAGE		READ INSTRUCTIONS BEFORE COMPLETING FORM
1. REPORT NUMBER MEMORANDUM REPORT BRL-MR-3415	2. GOVT ACCESSION NO. AD-A149984	3. RECIPIENT'S CATALOG NUMBER
4. TITLE *(and Subtitle)* An Orthogonal Grid Technique for Studying Internal Deformation and Energy Absorption in Target Penetration		5. TYPE OF REPORT & PERIOD COVERED 6. PERFORMING ORG. REPORT NUMBER
7. AUTHOR(s) William J. Bruchey and Jeffery T. Glass		8. CONTRACT OR GRANT NUMBER(s)
9. PERFORMING ORGANIZATION NAME AND ADDRESS U.S. Army Ballistic Research Laboratory ATTN: AMXBR-TBD Aberdeen Proving Ground, MD 21005-5066		10. PROGRAM ELEMENT, PROJECT, TASK AREA & WORK UNIT NUMBERS
11. CONTROLLING OFFICE NAME AND ADDRESS US Army Ballistic Research Laboratory ATTN: AMXBR-OD-ST Aberdeen Proving Ground, MD 21005-5066		12. REPORT DATE DECEMBER 1984 13. NUMBER OF PAGES 38
14. MONITORING AGENCY NAME & ADDRESS*(if different from Controlling Office)*		15. SECURITY CLASS. *(of this report)* Unclassified 15a. DECLASSIFICATION/DOWNGRADING SCHEDULE

16. DISTRIBUTION STATEMENT *(of this Report)*

Approved for public release; distribution unlimited.

17. DISTRIBUTION STATEMENT *(of the abstract entered in Block 20, if different from Report)*

18. SUPPLEMENTARY NOTES

19. KEY WORDS *(Continue on reverse side if necessary and identify by block number)*

Ballistics, armor, penetrator, materials, plastic, deformation

20. ABSTRACT *(Continue on reverse side if necessary and identify by block number)*

An experimental technique was developed using a split target and internal grid to study material deformation and flow as a result of penetration. Data taken before and after impact show changes in hardness profiles and also the strain distribution within the target. Energy balances equations were developed and showed that over 90% of the incoming energy of the penetrator can be accounted for by the strain energy in the penetrator and target material.

DD FORM 1 JAN 73 1473 EDITION OF 1 NOV 65 IS OBSOLETE

UNCLASSIFIED

SECURITY CLASSIFICATION OF THIS PAGE *(When Data Entered)*

TABLE OF CONTENTS

LIST OF ILLUSTRATIONS

I. BACKGROUND

The measurement of plastic strain has long been of interest to engineers and scientists concerned with the behavior of materials subjected to impact loading, such as experienced when a kinetic energy projectile impacts an armor target. Many methods have been devised to measure the strains experienced in materials subject to loads in excess of the yield limit, but these methods have usually been restricted to conditions of low rates of loading. With the rapid escalation of threats within the field of armor and penetrator ordnance, the researcher is being pressed to expand the understanding of penetrator - target interaction to permit the development of new, improved ordnance.

For the study of the mechanics of deformation it is necessary to be able to measure the strain and energy absorption occurring everywhere within the zone of deformation. In many penetration experiments, these zones of deformation may be quite small while the levels of strain are quite high. A prerequisite for the measurement of the strain sustained by an element passing through the deformation zone is a knowledge of the precise size, shape, and position of that element before entry to the plastic field.

To study the strain distribution and energy distribution within an impacted target, a technique was developed for depositing an orthogonal grid on an internal surface of the target. Measurements of both total strain and strain increments could then be made and then used to determine energy absorption anywhere within the zone of deformation.

The work presented here deals with the specific case of long rod penetration into semi-infinite rolled homogeneous armor (RHA) steel targets. Previous work most closely paralleling this study was performed by Mobley, Dietrich, Harrison, Pond, and Glass.[1] Their studies utilized the phenomenon of strain hardening to correlate strain and change in microhardness in order to obtain an energy balance for pellets impacting aluminum, copper, and mild steel semi-infinite targets. Energy balances were obtained utilizing the concept of the Prager curve, which will be described in more detail later. Mobley utilized the same correlation technique in his dissertation[2] for notched and unnotched impact specimens, deformed through a wide range of velocities. He determined "critical velocities" for the material as well as demonstrating the effects of strain localization in his specimens. Pond and Hsu[3] then refined the determination of strain in a target by placing a

---

[1] *R. B. Pond, C. Mobley, C. M. Glass, "Energy Balances in Hypervelocity Penetration," Proceedings of the Sixth Symposium on Hypervelocity Impact, Vol. 2, Part 2 (1963); and C. Mobley, A. M. Dietrich, E. Harrison, R. B. Pond, The Effect of Metal Properties on Hypervelocity Penetration, "Summary Report," U.S. Army Contract No. DA-36-034-ORD-3565 RD.*

[2] *C. Mobley, Ph.D. dissertation, The Johns Hopkins University, "The Effect of Velocity on the Deformation of Modified Charpy Copper Specimens," 1968.*

[3] *N. Hsu, R. Pond, "Hypervelocity Target Dynamics as Seen by Three-Dimensional Markers," AIAA Hypervelocity Impact Conference (1969).*

three-dimensional array of wires in copper targets prior to hypervelocity pellet impact and measuring their displacements after impact. Variations of the above techniques were utilized in the current study which involves a semi-infinite RHA steel target undergoing penetration by a tungsten-nickel-iron alloy penetrator.

II. INTRODUCTION

The traditional approach to armor and penetrator design for ordnance applications has followed two paths. In the area of penetrators, the approach has been to increase muzzle velocities, increase the penetrator density, and increase the length to diameter ratio of the penetrator. In the area of armor design, effectiveness has been enhanced by increasing the hardness of the armor steel and its thickness. This has largely been a brute force approach to ordnance design. However, penetrators are now reaching the design limits of the gun systems used to launch them, and armored vehicles are approaching the design limits of bridges and roads over which they must travel. Under these constraints, it has become necessary to re-emphasize the development of materials with "new or unique" properties to withstand the severe stresses imposed during ballistic impact.

In the past, high velocity deformation was often considered hydrodynamic in nature and independent of material parameters, such as microstructure, crystallography, etc. Experimental studies have shown this concept to be incorrect.[4-7] Consequently, if one is to design advanced ordnance, then a more detailed and faithful characterization of the materials being used must be undertaken. The objective of this program was to gain additional insight into the interaction between the penetrator and target during the penetration of a semi-infinite block of target material. The experimental efforts were designed to provide data on the energy partitioning between the penetrator and impacted target and to provide an uncomplicated geometrical configuration which would lend itself to simulation by numerical modeling. To obtain this information, it is necessary to observe the material flow and energy dissipation process in an opaque material. Although experiments have been conducted in transparent materials, such as wax and plexiglass, the applicability of these results is ambiguous when one

---

[4] *H. P. Tardiff, F. Claisse, P. Challet, Some Observations on Explosively Loaded Iron and Mild Steel, "Response of Metals to High Velocity Deformation," Conf. Metal. Soc., 9, 389 (1961).*

[5] *R. B. Pond, C. M. Glass, Crystallographic Aspects of High Velocity Deformation of Aluminum Single Crystals, "Response of Metals to High Velocity Deformation," Conf. Metal. Soc., 9, 145 (1961).*

[6] *G. L. Moss, S. Toms, R. Vitali, A. Merendino, "Effect of Target Microstructure on Penetration by Shaped Charge Jets," BRLM Report No. 1739 (April 1966). (AD# 487842)*

[7] *C. M. Glass, G. L. Moss, S. K. Golaski, Effects of Explosive Loading on Single Crystals and Polycrystalline Aggregates, "Response of Metals to High Velocity Deformation," Conf. Metal. Soc., 9, 115 (1961).*

considers the high strength materials used in most ordnance applications. Another requirement is to be able to represent the effects of strain rate and high stresses on the material properties. A method initially proposed by Prager[8] and utilized in subsequent high velocity experiments was used to address this problem.

III. TEST TECHNIQUES

Based on previous small-scale experimentation at the Ballistic Research Laboratory, testing was conducted using long rod penetrators which had a length-to-diameter ratio of 10 and a mass of 65 grams. The penetrator geometry was that of a right circular cylinder with a hemispherical nose. There has been a considerable data base collected using this geometry penetrator, and it was felt that its continued use in this program would allow the expansion of this data base and permit the use of the data gathered in this program to be used to explain some of the phenomena observed in other firing programs. Each of the penetrators tested was fired at a muzzle velocity of 1550 meters/second. The targets were either 15 cm cubes of RHA or the split target composed of a RHA core split on a plane parallel to the shot line and held together in a 4340 steel sleeve. Photographs of the split target configuration are shown in a later section. Figure 1 shows a sketch of the experimental setup used during the conduct of these tests.

IV. METALLOGRAPHY

A. Semi-Infinite Target Blocks.

Sectioned targets were examined with both optical and electron microscopes. Various etchants were used, but the best results were obtained with Nitol and Picrol. The target material, RHA, whose nominal composition is listed in Table 1, was in the form of six-inch thick, rolled plate before being cut into cubes approximately 15 cm on each edge. (All targets were this geometry except the split target, whose configuration is discussed later). It should be noted that RHA is purchased by the U.S. Army on the basis of performance specifications rather than chemical compositions thereby resulting in significant chemical and/or microstructural differences from lot-to-lot.

TABLE I. Typical Chemistry For 15 cm Thick RHA Steel

C	Mn	P	S	Si	Ni	Cn
.22	.15	.025 max	.025 max	.15	3.2	1.2

[8] *W. Prager, "On Isotropic Materials with Continuous Transition from Elastic to Plastic State," Intern. Congr. Appl. Mech., 5th (1933).*

The RHA examined in this study consisted of a fine structure composed largely of bainite and tempered martensite (Fig. 2). Lighter regions, comparable to free ferrite in a plain carbon steel, were also seen with fine carbides scattered throughout the micro-structure. Due to the complexity of the alloying constituents, this initial study did not attempt to identify the exact compositions of the various phases.

An interesting characteristic of the microstructure of this RHA is shown in Figure 3. Spheroidal pockets of material can be seen to have been pulled out of the matrix material during polishing. If care is taken to retain these regions, they are found to etch more readily in Picrol than the matrix, indicating higher carbon content, and contain more than one phase at higher magnifications (Fig. 4). These areas were apparently a solid solution which spheroidized during heat treatment. The components in these regions did not have time to disperse during cooling and were precipitated as small, irregular particles inside some matrix material, all within the original spheroid upon passing through what was probably a eutectoid of some kind. Their frequency was fairly constant throughout the section (both close to and far away from penetration crater), and they are believed to be relatively hard regions due to the lack of distortion they underwent very near to the crater (Fig. 3). The matrix material, on the other hand, underwent severe deformation close to the crater, as can be seen by the elongated phases (Fig. 5). This deformation was very localized, however, and farther than approximately 0.37 millimeters away, no flow was apparent in the microstructure. In upper regions of the target (approximately the upper third), deformation adjacent to the crater was so severe that adiabatic shear bands (Fig. 6) and microcracks (Fig. 7) were formed. It is believed that the higher pressure and greater material flow associated with the region just beyond projectile entry and prior to its degradation are responsible for the shear band and microcrack formation.

Targets were also macroetched with a hot 50% concentrated hydrochloric acid etch for 15 to 30 minutes. This procedure revealed an area of reverse flow (against penetrator flight direction) near the upper surface, a region of mixed flow, and finally an area of flow approximately parallel to flight direction (Fig. 8). In the region near the entry surface where gross deformation is in the reverse direction, there is actually a thin layer of parallel flow adjacent to the crater. It is in this thin layer that the microcracks and adiabatic shear bands, both oriented in the same direction as the layer, were formed. No localized shear bands or cracks were seen below the mixed flow region (i.e. they were located, as previously stated, in the upper regions of the target, nearer to penetration entry surface).

Hardness profiles of sectioned targets following penetration revealed, as expected, a higher hardness near the crater due to strain hardening. Both microhardness and Rockwell C hardness measurements were taken in order to make a comparison. Microhardness has the advantage of small impressions and can therefore be used very close to the crater edge but becomes too dependent on micro-constituents a short distance away, causing large variations in the readings. Rockwell C cannot probe close to the crater but averages over larger areas than the microhardness measurements, giving good general trends (Fig. 9). The results for one-half (longitudinally) of a sectioned surface can be seen in the three-dimensional plot made from a grid of hardness measurements (Fig. 10). These hardness readings are not changes

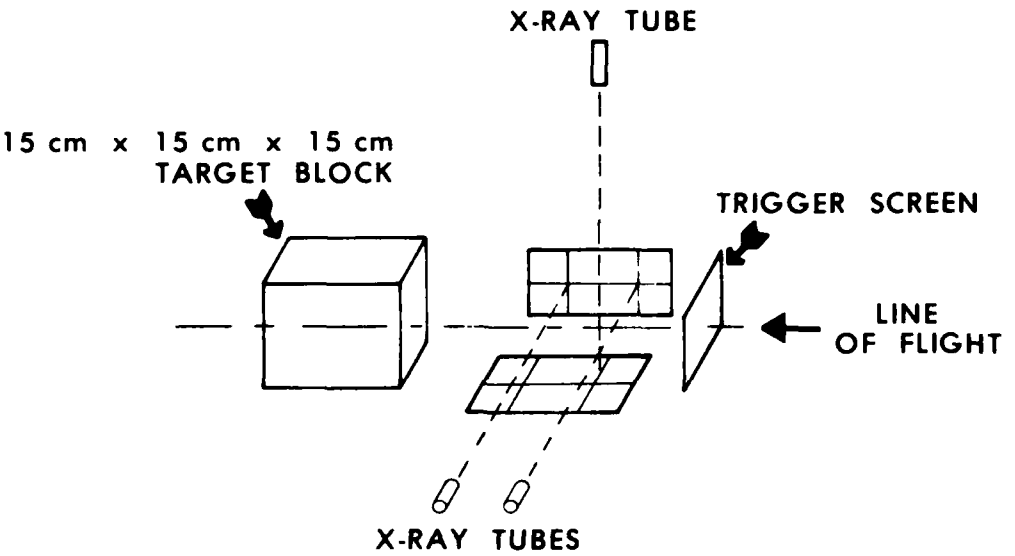

Figure 1. Sketch of Experimental Test Set-up.

Figure 2. Photograph of Undeformed RHA Microstructure. Nitol Etch, 300X.

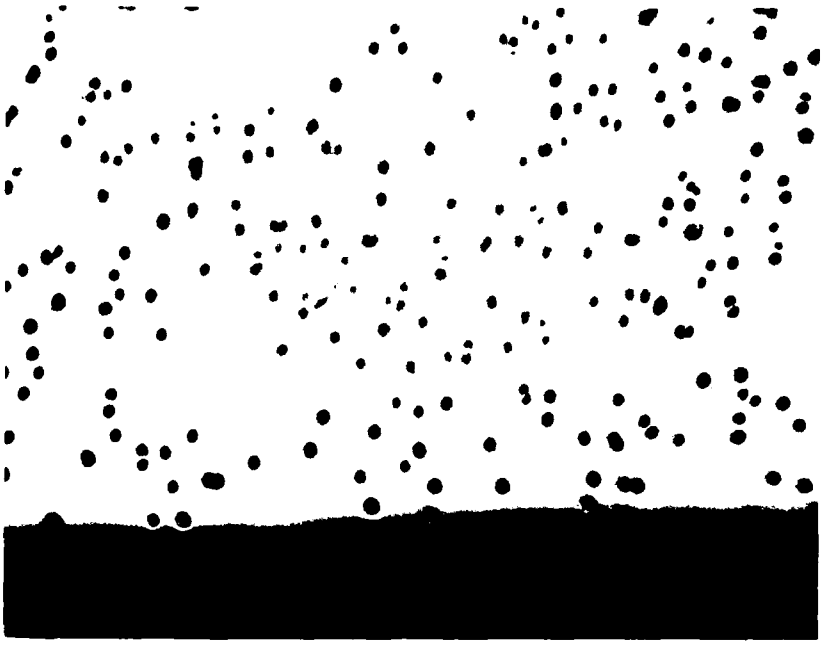

Figure 3. Spheroidal Regions in the RHA Microstructure Removed During Polishing. Unetched, 55X.

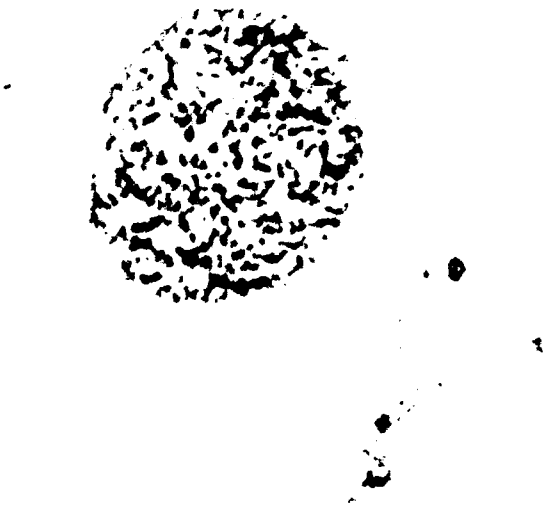

Figure 4. Higher Magnification Image of Figure. Picral etch, 2640X.

Figure 5. Target Microstrcture Near Penetration Crater (Crater is Oriented Parallel to Focused Portion of Photo). Nitol Etch, 800X.

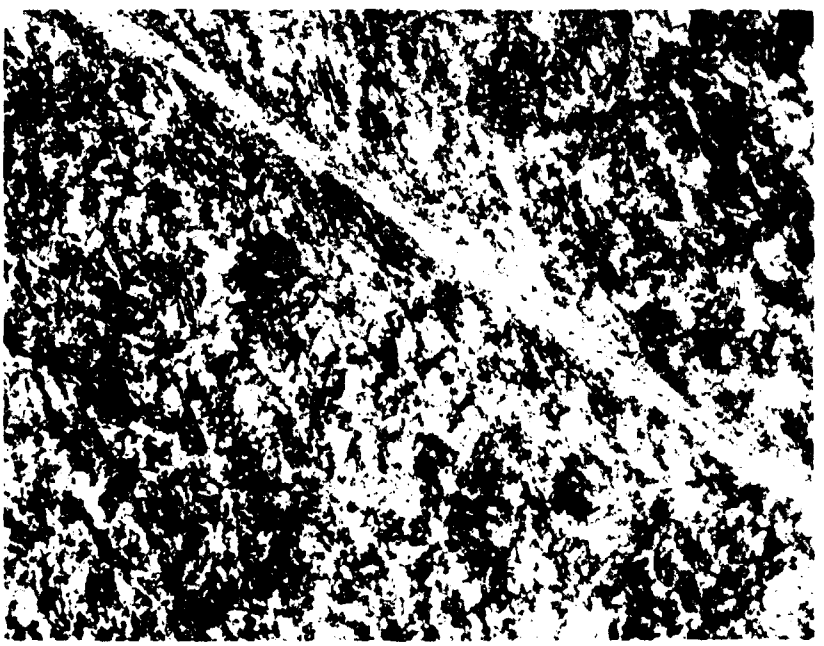

Figure 6. Adiabatic Shear Bands Formed During Penetration. Nitol Etch, 320X.

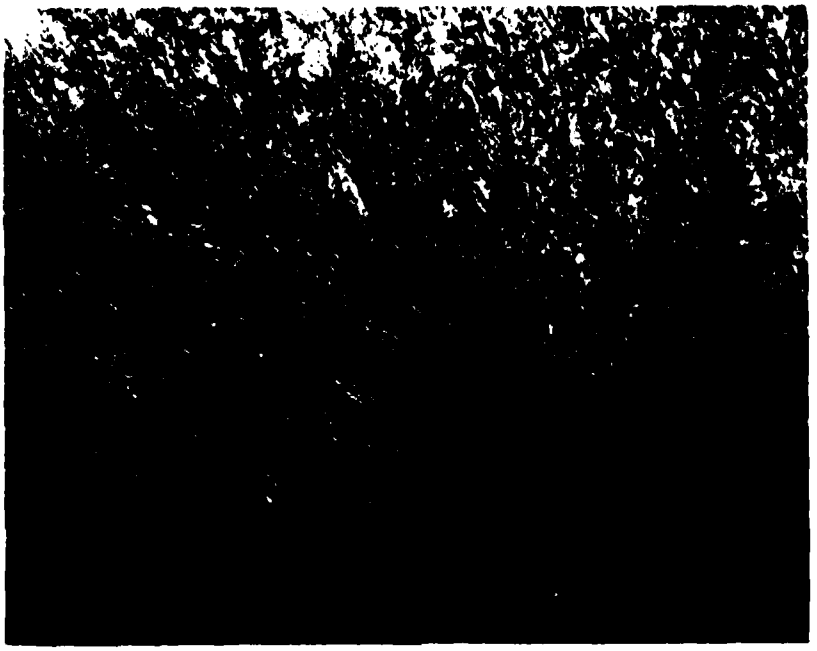

Figure 7. Tip of Microcrack and Localized Shear. Nitol Etch, 280X.

Figure 8. Macroetched Section of Target Revealing Flow Pattern Caused by Impact. Hot HCℓ Etch.

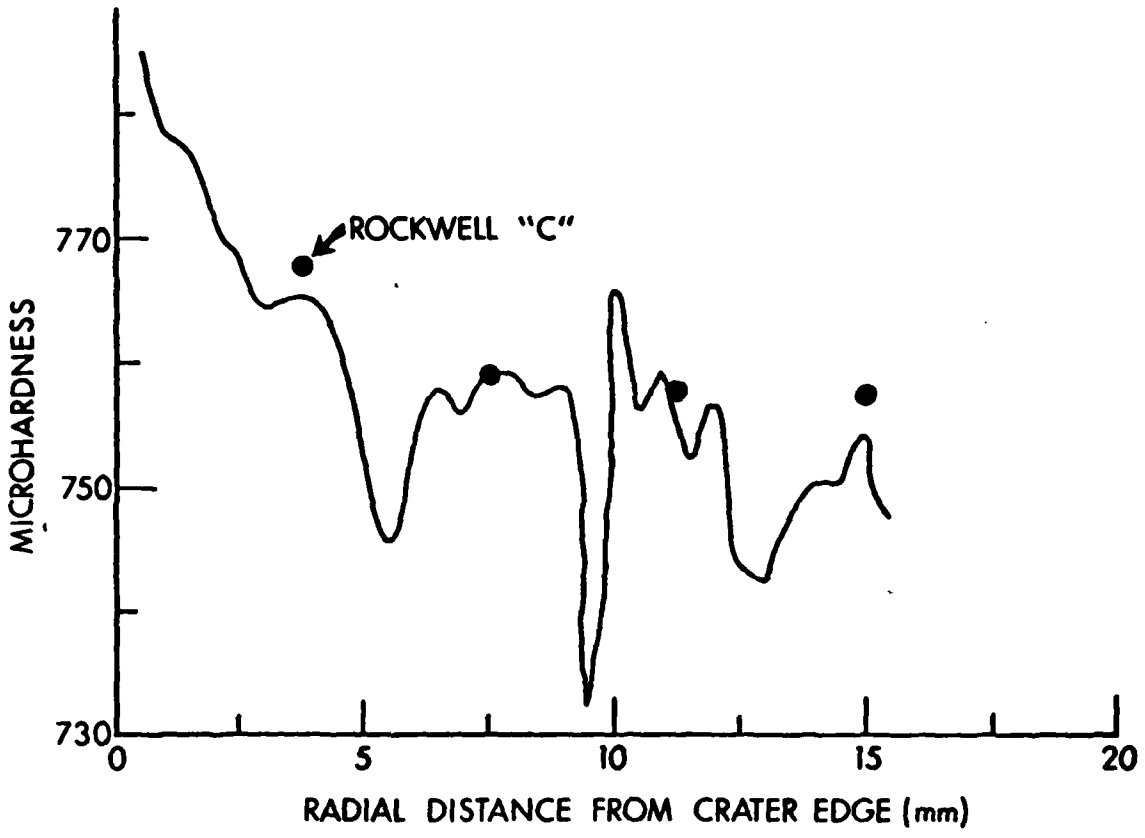

Figure 9. Hardness Contours Across Target Block. Rockwell C and Micro-Hardness.

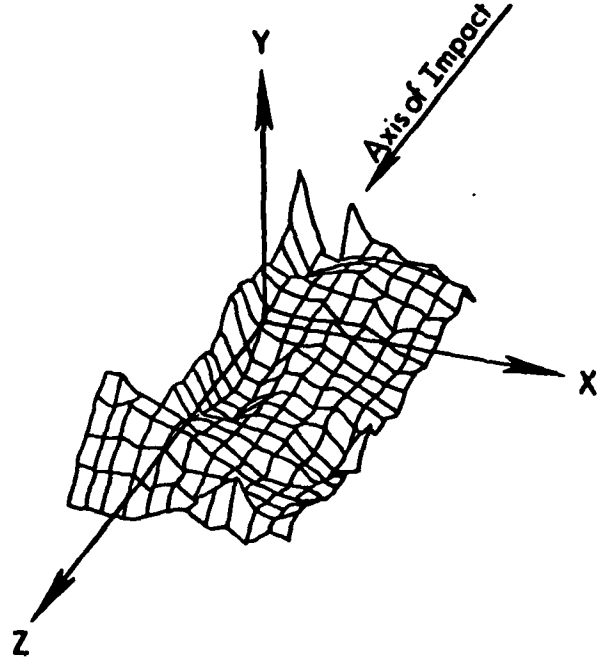

Figure 10. Three-Dimensional Hardness Contours Across a Sectioned Target.

in hardness but rather nominal hardness after penetration, giving rise to inaccuracies due to local variations in hardness before penetration. The hardness change would be much more pertinent. One should also keep in mind that the physical significance of the increased hardness is somewhat ambiguous. Although it is related to stored energy (i.e. dislocations generated, etc.) in some way, which is in turn related to strain, the quantitative relationship is not a simple problem. A phenomenon known as strain softening has even been documented for certain materials under given loading conditions. On the other hand, excellent energy balances have been obtained in copper and aluminum targets by relating hardness values to strain via a uniaxial tensile test and then integrating this strain to determine strain energy.[1] This was attempted with RHA, however, no accurate hardness changes could be measured prior to necking, making a hardness change, strain energy correlation very difficult. This was due to the different strain hardening characteristics and the lower ductility of RHA as compared to the copper and aluminum successfully used in previous studies. It was therefore necessary to directly determine the strain field and thereby strain energy in the target by the method described in the next section.

B. Split Target.

The preceeding work on solid target blocks was done on post shot target sections and required no special considerations as far as target preparation was concerned. The quantitative information it generates, without more complete background data, is limited. A technique which would allow unambiguous internal mapping of material flow due to penetration into RHA targets would not only help to further generate understanding of the process of long rod penetration, but would also allow for more quantitative data to be obtained from targets already tested, once the proper correlations are derived. For example, if one could derive the hardness change/strain energy relationship in a specially designed target, it could be utilized in the post shot analysis of targets for which only hardness data is available. A unique split target system was developed which allowed hardness changes and material flow to be measured (i.e. before and after) on a radial plane through the crater. This was accomplished by machining a cylindrical target split down its longitudinal axis, which fit into a mating, unsplit sleeve or constraining ring,to hold the target together during penetration. The target and sleeve were machined with a slight interference fit and taper (approximately one degree). The large ends were situated towards the incoming projectile. A front plate bolted to the face of the sleeve prevented any back slipping of the target out of the sleeve during target impact (Fig. 11 & 12). The penetrator was fired parallel and directly into the split plane such that after firing, the longitudinal axis of the crater laid in the split plane.

Prior to firing, hardness measurements were taken over the entire split surface. This allowed the change in hardness to be determined while the marks left by the indentation measurements could be used as a reference grid to determine material flow (Fig. 13). The change in hardness is shown as iso-hardness contours (Fig. 14). Note the pockets of high hardness in the upper regions of the target adjacent to the crater. These correlate roughly with the regions of mixed flow and adiabatic shear banding observed in the metallographic examination of post shot sections of other targets. Another interesting observation is the negative change in hardness in the outer

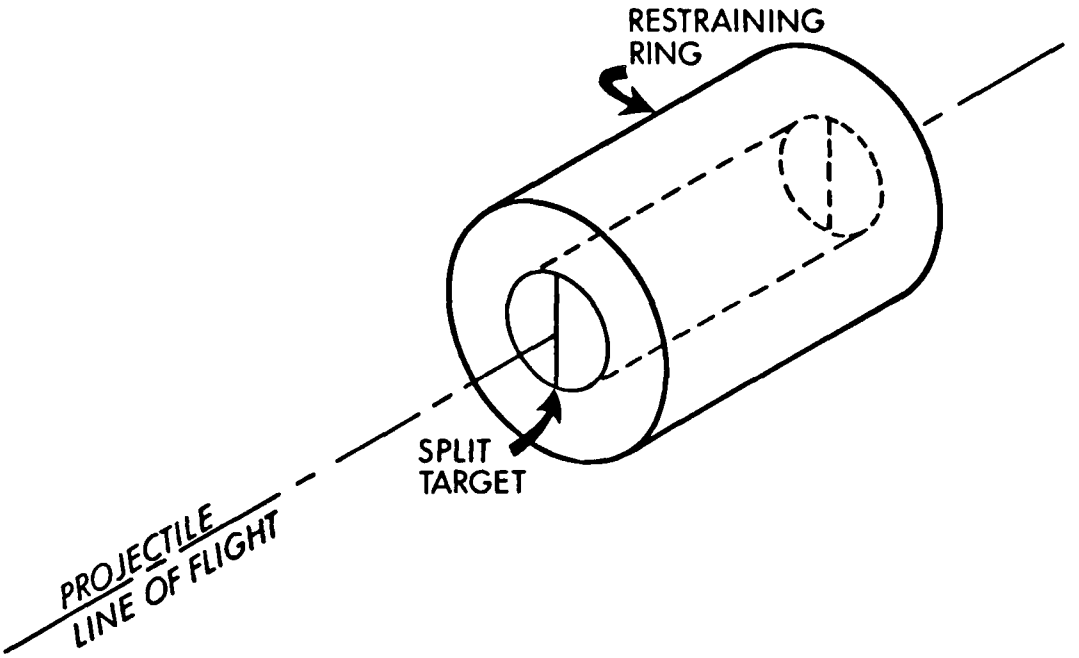

Figure 11. Schematic of Gun and Split Target.

Figure 12. Photograph of Split Target Assembly.

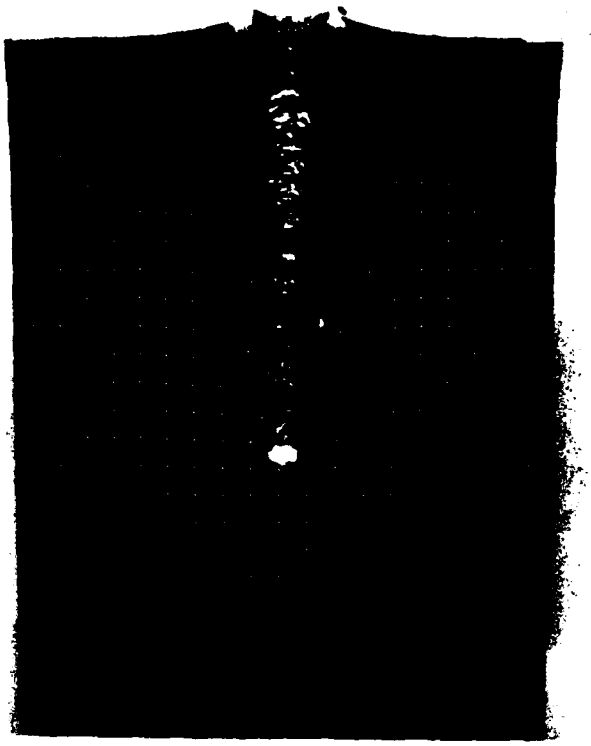

Figure 13. Photograph of Hardness Indentations.

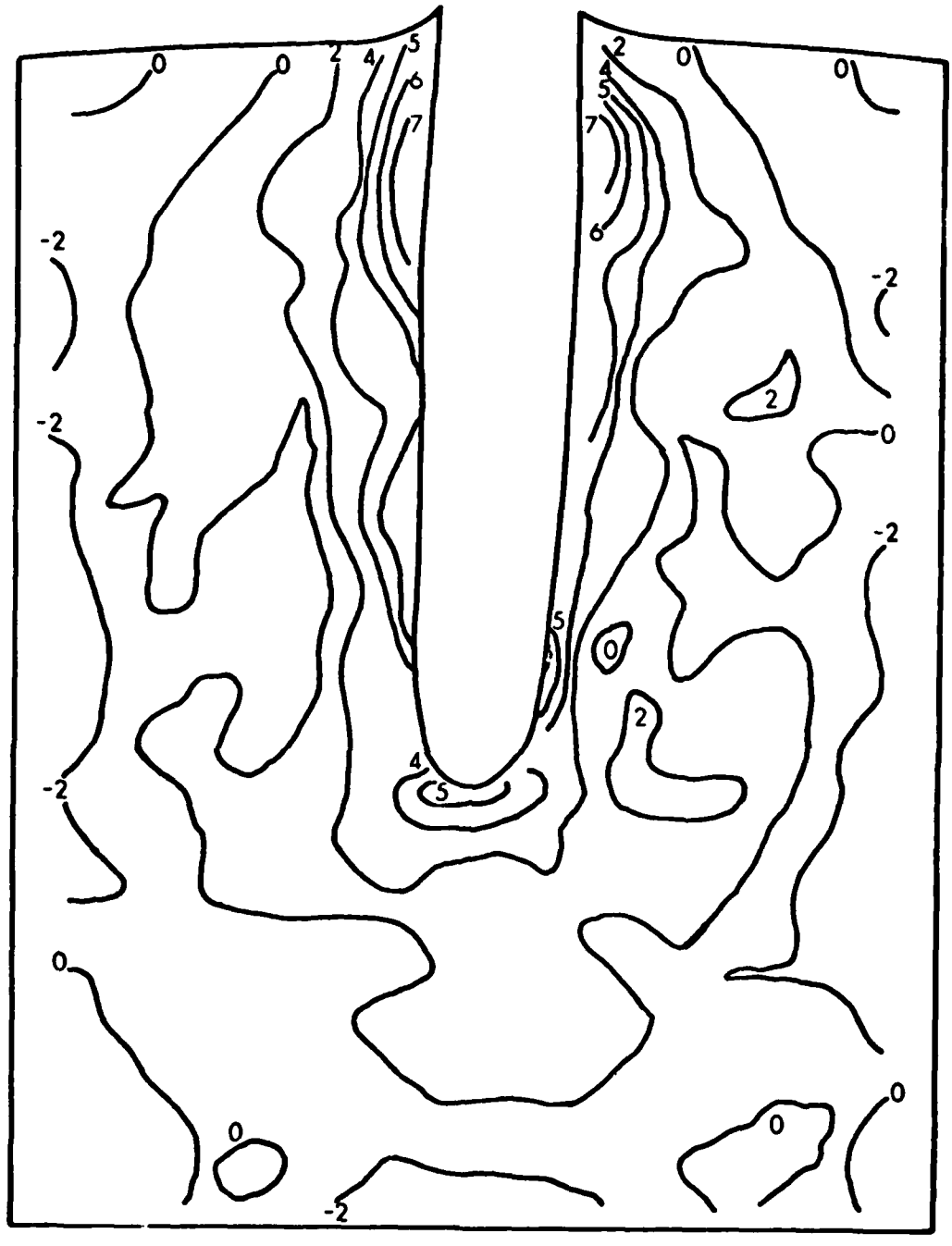

Figure 14. Hardness Change After Impact.

regions of the target. This "strain softening" pattern (zero hardness change contour and outward) is believed to be connected with wave propagation and reflection from target edges. More experiments are necessary, however, to determine its reproducibility before an exact mechanism is offered.

As previously mentioned, indentation formed by the hardness measurements were used as a reference grid to determine strain in the target. An optical comparator was used to measure the locations of these indentations both before and after penetrations, from which displacements were calculated. The results are shown in Figure 15. Line segments in this plot connect equivalent points before and after penetration. The larger circles at one end of each segment indicate the post shot location. Note the flow pattern indicated on this plot: away from the crater and towards the upper free surface. Regions of large displacement (i.e. near the front surface) do not necessarily indicate greatest energy absorption. Relative displacements, or strain, as explained before, are responsible for this. Another interesting observation is the lack of displacement near the tip of the crater. The material is not so near a free surface as at the entry point and is therefore not able to flow as readily. It is probably loaded in compression in this region with much larger residual stresses than in the upper region where flow occurred.

From the displacements discussed above, the strain at each point may be calculated. Assuming axial symmetry about the penetration axis, it can be shown that the components of strain are:

$$e_{RR} = \frac{1}{2} \quad r_R^2 + z_R^2 - 1 \tag{1}$$

$$e_{\phi\phi} = \frac{1}{2} \quad \frac{r^2}{R^2} - 1 \tag{2}$$

$$e_{ZZ} = \frac{1}{2} \quad r_Z^2 + z_Z^2 - 1 \tag{3}$$

$$e_{RZ} = e_{ZR} = \frac{1}{2} (r_Z r_R + z_Z z_R) \tag{4}$$

$$e_{R\phi} = e_{\phi R} = e_{Z\phi} = e_{\phi Z} = 0, \tag{5}$$

where r = radial location before penetration
R = radial location after penetration
z = vertical location before penetration
Z = vertical location after penetration

$$r_R = \frac{\partial r}{\partial R} ; \quad r_Z = \frac{\partial r}{\partial Z} ; \quad z_R = \frac{\partial z}{\partial R} ; \quad z_Z = \frac{\partial z}{\partial Z} . \tag{6}$$

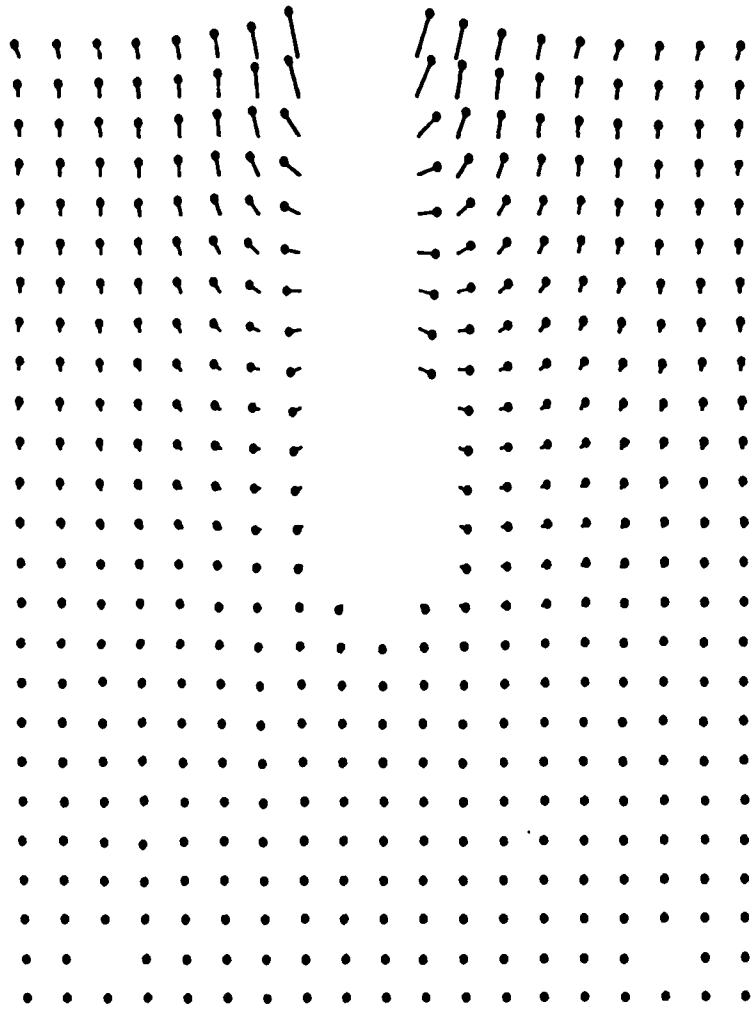

Figure 15. Displacement Plot of Hardness Indentations After Impact.

From these elements of the strain tensor, the strain invariants are found to be:

$$I_1 = e_{RR} + e_{\phi\phi} + e_{ZZ} \tag{7}$$

$$I_2 = \begin{vmatrix} e_{\phi\phi} & 0 \\ 0 & e_{ZZ} \end{vmatrix} + \begin{vmatrix} e_{ZZ} & e_{ZR} \\ e_{RZ} & e_{RR} \end{vmatrix} + \begin{vmatrix} e_{RR} & 0 \\ 0 & e_{\phi\phi} \end{vmatrix} \tag{8}$$

$$= e_{\phi\phi}\, e_{ZZ} + e_{ZZ}\, r_{RR} - e_{RZ}^2 + e_{RR}\, e_{\phi\phi}$$

$$I_3 = \det \left| e_{1k} \right| \tag{9}$$

$$= -e_{rz}^2\, e_{\phi\phi}.$$

Each invariant was calculated at each grid point and iso-invariant contour plotted for I_1 and I_2 (Fig. 16 and 17, respectively). I_3 was found to be zero everywhere in the section within experimental error. In the infinitesimal limit, I_1 is proportional to a volume change and I_2 to a shear strain. For finite deformations, as in this case, higher order terms become more significant, making the physical meanings of the invariant less clear but still related to the infinitesimal case. Note the close relation between invariant and hardness contours (Figs. 14, 16, and 17) for the regions of greatest material flow in pockets adjacent to the crater in the upper portions of the target. Near the crater tip, however, the strain has not reached the values indicated by hardness. This suggests that the hardness may have increased due to increased stored energy (i.e. dislocation generation, etc.) perhaps brought about by shock wave propagation in this region rather than any macroscopic strain. It should be noted, however, that the stored energy and strain are related and that hardness increase in the upper portion of the target is also due to stored energy which follows the macroscopic strain due to loading conditions and material flow.

V. ENERGY BALANCE

Although the strain field can be determined by the method described above, additional information is necessary to calculate an energy balance. To accomplish this, a method first described by Prager[8] was employed. As is well known, the energy absorbed per unit volume by a material during tensile deformation is given by the area under its true stress-true strain curve. As the rate of deformation is increased in such a test, it is found that the yield and ultimate strengths begin to converge to the true fracture strength of the material. A dynamic true stress-true strain tensile curve can therefore be defined by extending the elastic portion of the quasi-static curve up to the true fracture stress and then drawing a horizontal line over to the fracture strain. This has been done for the RHA target material and the tungsten penetrator material (Figs. 18 & 19).

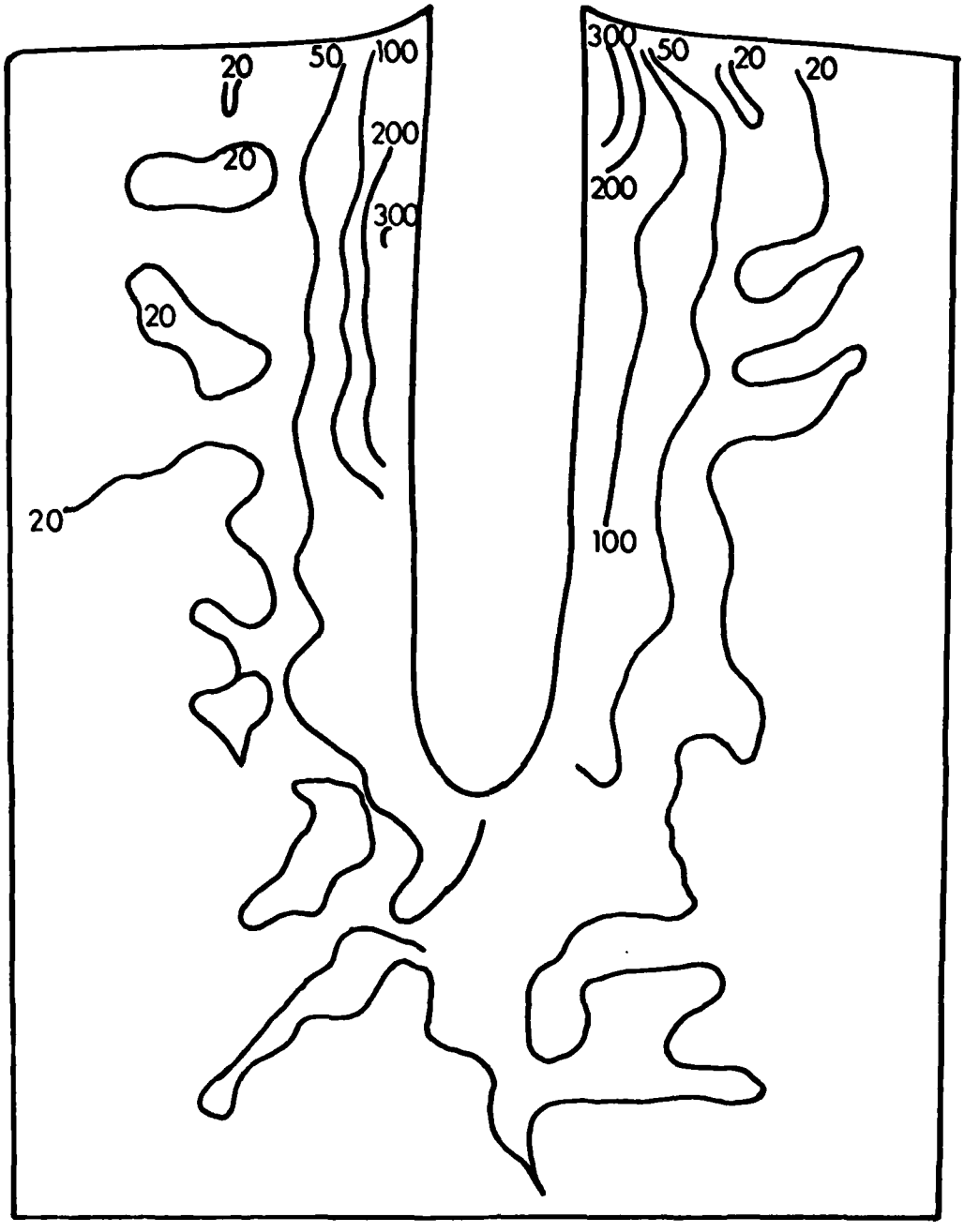

Figure 16. Iso-Invariant Mapping of the First Invariant of the Strain Tensor-($I_1 \times 10^{-4}$).

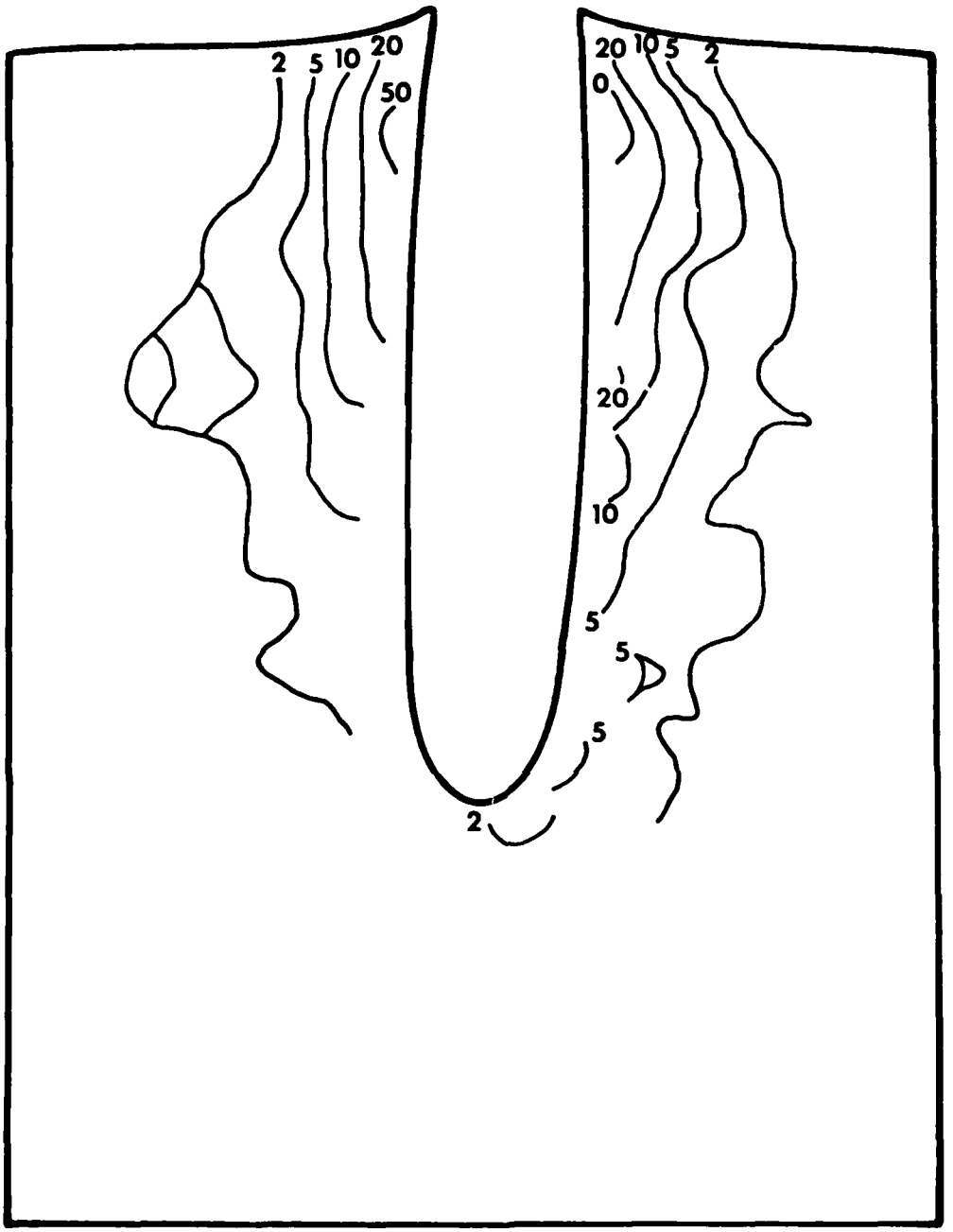

Figure 17: Iso-Invariant Mapping of the Second Invariant of the Strain Tensor - ($I_2 \times 10^{-3}$).

This concept was used previously in the treatment of high velocity impact,[1] high velocity metal extrusion,[9] and high velocity metal cutting.[10] The hypothesis is that the material is being deformed faster than it can strain harden. The area under the elastic portion of the dynamic curve represents the energy necessary to initiate metal flow. This energy must be added more quickly than Prager's proposed "time delay" for strain hardening. Once the metal begins to flow, it will continue to do so until one of three things occurs: the energy is dissipated, the material fractures, or the time delay for strain hardening is reached. Remaining energy will be absorbed by areas adjacent to the crater in the form of a change in structure or as residual stress (stored energy). An objection to this method of analysis is brought about by tests conducted in uniaxial tension/compression at high strain rates. In these tests, one sees the increase in yield with strain rate but also a corresponding decrease in ductility. It is believed that this is due to the localization of strain under the non-hydrostatic test conditions whereas crater formation occurs under high hydrostatic pressures and consequently the ductility remains relatively constant. The quasi-static true tensile strain to fracture is therefore believed to be more indicative of the strain which occurs before fracture or "material separation" during crater formation. The ductility may, in fact, increase slightly during the penetration process since the role of inclusions and other defects is most likely minimized by the hydrostatic pressures and high velocities. For the present work, the true strain to fracture from quasi-static tests was assumed to be within experimental error of the actual value.

Employing this method, the dynamic curves for the target and penetrator material were determined (Figs. 18 & 19). The strain in these plots, which is obtained from the test as true longitudinal strain, must now be related to the invariants of the strain tensor in order to obtain the strain energy in the targets. Assuming that tensile deformation is a constant volume phenomena, the longitudinal strain - strain invariant relationship can be calculated for a uniaxial tensile test.

Assuming axial symmetry, it can be shown that the components of the strain tensor become:

$$e_{RR} = \frac{1}{2}\left(\exp\left(-\varepsilon_{\ell}\right)-1\right) \tag{10}$$

$$e_{ZZ} = \frac{1}{2}\left(\exp\left(2\varepsilon_{\ell}\right)-1\right) \tag{11}$$

$$e_{\phi\phi} = \exp\left(-\varepsilon_{\ell}\right)-1 \tag{12}$$

---

[9] *R. B. Pond, "Cold Extrude Rapidly to Produce Long, Thin-wall Aluminum Tubes," Metal Progr., 89, No. 6, 77 (1966) and unpublished results referred to in Ref. 2.*

[10] *D. C. Drucker, "Analogous Strain Rate Effects in Jet Formation and Metal Cutting," Tech. Rpt. No. 4, BRL Contract No. DA-19-020-ORD-3426 (August 1963).*

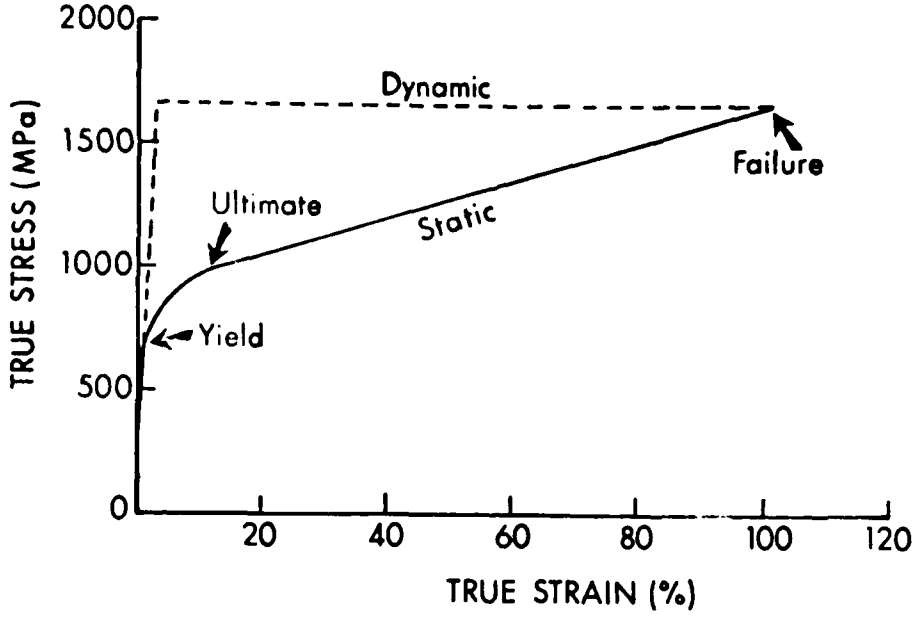

Figure 18. True Stress vs. True Strain for RHA Target Material.

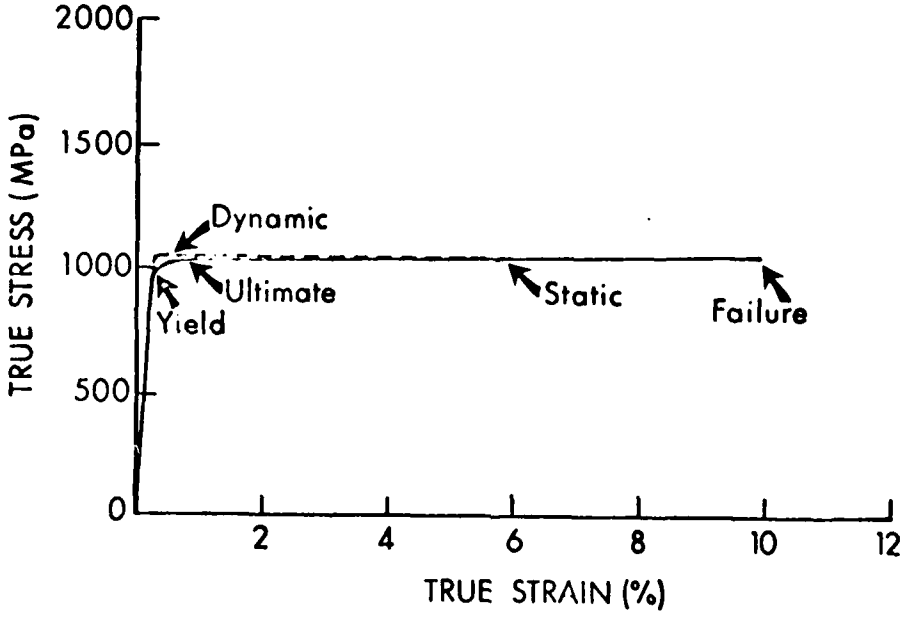

Figure 19. True Stress vs. True Strain for Tungsten Alloy Penetrator Material.

and the first and second invariants are:

$$I_1 = -2 + \frac{3}{4} \exp(-\varepsilon_\ell) + \frac{1}{2} \exp(2\varepsilon_\ell) \tag{13}$$

$$I_2 = \frac{5}{4} + \frac{3}{4} (\exp \varepsilon_\ell - \exp 2\varepsilon_\ell) - \frac{7}{8} \exp(-\varepsilon_\ell) + \frac{1}{2} \exp(-2\varepsilon_\ell), \tag{14}$$

where: e denotes engineering strain
ε denotes true strain.

The second invariant obtained for RHA is shown plotted against the longitudinal strain in Figure 19. The same was done for the first invariant but when the relationship was correlated with the iso-invariant plot from the target, the results were off by roughly a factor of four when compared to the second invariant. When the energy balance was then calculated with the first invariant more energy was returned than had actually been delivered to the target. This is consistent with plasticity theory in that the second invariant is representative of plastic deformation (shear strain), the first invariant, being indicative of a volume change. A quantitative reason for the large difference is unknown. It is perhaps related to the assumption of constant volume during tensile deformation. As can be seen in the invariant plots (Figs. 15 & 16). The contours of both are qualitatively the same. Future tests will continue to utilize both invariants in an attempt to determine the origin of the large difference.

A relationship between the energy absorbed during tensile deformation and the second invariant was obtained by cross plotting Figure 21 (the absorbed energy versus true longitudinal strain) and Figure 20 (the second invariant of the strain tensor versus true longitudinal strain). In this way the energy absorbed by the material when it has been strained to a given value (denoted by the second invariant) is known. This was only necessary for the RHA since the tungsten penetrator had its entire volume deformed to fracture judging from observations of the severe material flow. Its bulk was found to line the crater walls with a small residual amount at the crater tips, all being severely deformed. Therefore, only one energy absorption value is necessary - the amount absorbed to fracture - which can be taken directly from the Prager curve in Figure 19.

The energy balance now becomes

I. Impact Energy $= \frac{1}{2} MV^2$

$\cong$ 73,125 Joules

II. Energy After Impact

A. Projectile deformation energy

= penetrator volume x energy per unit volume to fracture for tungsten

$\cong$ 1,684 Joules

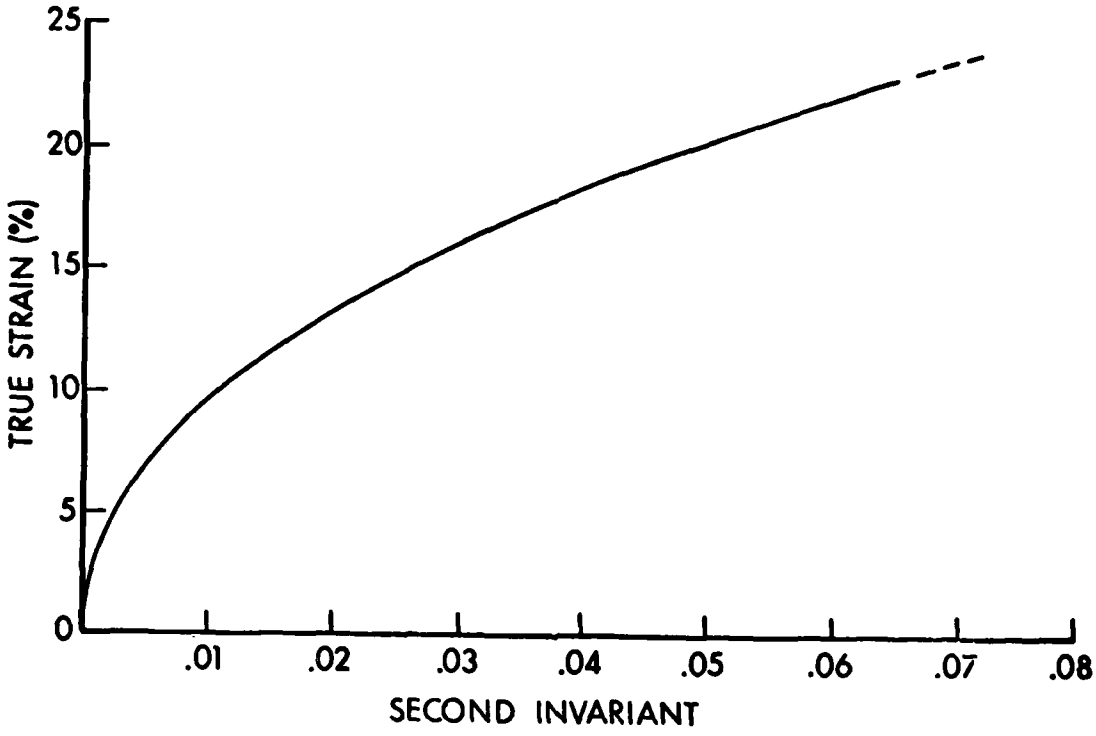

Figure 20. True Strain vs. Second Invariant of Strain For Uniaxial Tensile Deformation.

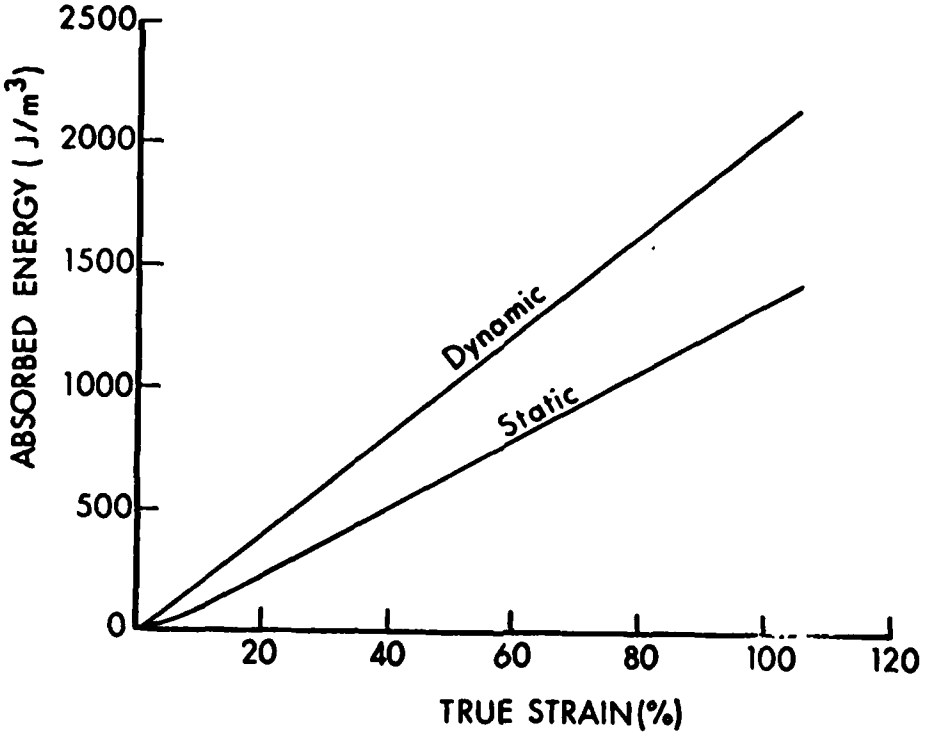

Figure 21. Absorbed Energy vs. True Strain For Uniaxial Tensile Deformation.

B. Crater formation energy

= volume of crater x energy per unit volume to fracture for RHA.

≅ 47,606 Joules

C. Strain energy in target

≅ 18,618 Joules .

(To obtain this target energy, volumes for various 2nd invariant values were approximated and multiplied by the appropriate energies per unit volume and final values summoned. In the future, test curves fitted to the invariants will be integrated over the appropriate energy values to obtain more accurate estimates.)

The final energy after impact is then

$$A + B + C = 67,909 \text{ Joules}$$

or 93% of the incoming projectile energy.

Approximately 93% of the incoming energy (a much larger fraction than nad been expected) is accounted for by the strain energy of the penetrator and target material, including crater formation. No material was assumed to disintegrate since total mass before and after penetration for the systems was constant. Energy not accounted for could be in such forms as (i) slight material disintegration, (ii) frictional heat, (iii) acoustic radiation, (iv) electro-magnetic radiation, etc.

VI. DISCUSSION AND CONCLUSION

The Prager concept of material deformation has been shown to describe ballistic impact at ordnance velocities, thus giving credibility to the approximation of elastic - perfectly plastic behavior of metals under constrained high velocity deformation. This phenomenon has been described in the past as a time delay for strain hardening. Although not attempted in the present work due to time and space considerations, it is felt a description of this phenomenon from a mechanistic standpoint is attainable. Separation of the roles of strain, strain rate, and high pressure in relation to this phenomenon are required before such a treatment is possible.

The projectile energy during the long rod penetration process has not only been shown to occur mainly in the strain of penetrator and target (including crater formation), but the distribution of this strain has also been determined. This distribution indicates that at initiation and termination of crater formation, there is relatively little strain. Refinement of a grid has recently been accomplished, thereby allowing more accurate strain field measurements for future work. This, coupled with experiments utilizing different velocities and penetrator materials, would increase the understanding of long rod penetration further. Stored energy (perhaps utilizing differential calorimetry) and temperature changes in

future tests should also be measured in order to independently verify the energy balance findings of this work. The temperature change will be generated by two separate sources; a latent heat of recrystallization, in which macroscopic flow mechanisms will be accounted for, and frictional heat. In order words, except for stored energy (i.e. elastic residual stresses, dislocations generated, etc.), all the macroscopic flow will manifest itself as heat. Therefore, although a distribution of temperature may not be possible, a check on the current energy balance could be obtained through fairly straightforward measurements of the total heat generated. The following equality is applicable:

Macroscopic Strain Energy = Heat Energy + Stored Energy - Frictional Heat.

Experiments involving heat measurements would therefore serve as excellent independent checks on the Prager Concept. The implications of the demonstration of this elastic-perfectly plastic behavior are dramatic, although systems in which it applys are unclear. As mentioned previously, for instance, dynamic tests under non-hydrostatic conditions do not find the ductility predicted from the Prager curve.

This split target configuration can also serve as an excellent check on computational codes. Experimental verification of internal deformation due to long rod penetration is possible, rather than simply using final crater shape. This provides a comparison between theory and experiment not often found.

This work also indicates that although hardness may be qualitatively indicative of strain, the correlation is far from exact as seen in the comparison of iso-invariant and iso-hardness plots. It would perhaps be more accurate to relate hardness and stored energy while continuing to measure strain by the split target method in future studies.

REFERENCES

1. R. B. Pond, C. Mobley, C. M. Glass, "Energy Balances in Hypervelocity Penetration," Proceedings of the Sixth Symposium on Hypervelocity Impact, Vol. 2, Part 2 (1963); and C. Mobley, A. M. Dietrich, E. Harrison, R. B. Pond, The Effect of Metal Properties on Hypervelocity Penetration, "Summary Report," U.S. Army Contract No. DA-36-034-ORD-3565 RD.

2. C. Mobley, Ph.D. dissertation, The Johns Hopkins University, "The Effect of Velocity on the Deformation of Modified Charpy Copper Specimens," 1968.

3. N. Hsu, R. Pond, "Hypervelocity Target Dynamics as Seen by Three Dimensional Markers," AIAA Hypervelocity Impact Conference (1969).

4. H. P. Tardiff, F. Claisse, P. Challet, Some Observations on Explosively Loaded Iron and Mild Steel, "Response of Metals to High Velocity Deformation," Conf. Metal. Soc., 9, 389 (1961).

5. R. B. Pond, C. M. Glass, Crystallographic Aspects of High Velocity Deformation of Aluminum Single Crystals, "Response of Metals to High Velocity Deformation," Conf. Metal. Soc., 9, 145 (1961).

6. G.L. Moss, S. Toms, R. Vitali, A. Merendino, "Effect of Target Microstructure on Penetration by Shaped Charge Jets," BRLM Report No. 1739 (April 1966). (AD# 487842)

7. C. M. Glass, G. L. Moss, S. K. Golaski, Effects of Explosive Loading on Single Crystals and Polycrystalline Aggregates, "Response of Metals to High Velocity Deformation," Conf. Metal. Soc., 9, 115 (1961).

8. W. Prager, "On Isotropic Materials with Continuous Transition from Elastic to Plastic State," Intern. Congr. Appl. Mech., 5th (1933).

9. R. B. Pond, "Cold Extrude Rapidly to Produce Long, Thin-wall Aluminum Tubes," Metal Progr., 89, No. 6, 77 (1966) and unpublished results referred to in Ref. 2.

10. D. C. Drucker, "Analogous Strain Rate Effects in Jet Formation and Metal Cutting," Tech. Rpt. No. 4, BRL Contract No. DA-19-020-ORD-3426 (August 1963).

DISTRIBUTION LIST

No. of Copies	Organization
12	Administrator Defense Technical Info Center ATTN: DTIC-DDA Cameron Station Alexandria, VA 22314
2	Director Defense Advanced Research Projects Agency ATTN: Tech Info Dr. E. Van Reuth 1400 Wilson Boulevard Arlington, VA 22209
1	Deputy Assistant Secretary of the Army (R&D) Department of the Army Washington, DC 20310
1	HQDA (DAMA-ARP-P, Dr. Watson) Washington, DC 20310
1	HQDA (DAMA-ART-M) Washington, DC 20310
1	HQDA (DAMA-MS) Washington, DC 20310
1	Commandant US Army Command and General Staff College ATTN: Archives Fort Leavenworth, KS 66027
1	Commander US Army War College ATTN: Lib Carlisle Barracks, PA 17013
1	Commander US Army Materiel Development and Readiness Command ATTN: AMCDRA-ST 5001 Eisenhower Avenue Alexandria, VA 22333
1	Commander Armament R&D Center US Army AMCCOM ATTN: SMCAR-TDC Dover, NJ 07801
5	Commander Armament R&D Center US Army AMCCOM ATTN: SMCAR-TSS SMCAR-LCA, T. Davidson SMCAR-SC, J. D. Corrie J. Beetle E. Bloore Dover, NJ 07801
1	Director Benet Weapons Laboratory Armament R&D Center US Army AMCCOM ATTN: SMCAR-LCB-TL Watervliet, NY 12189
1	Commander US Army Armament, Munitions and Chemical Command ATTN: AMSMC-LEP-L Rock Island, IL 61299
6	Director Benet Weapons Laboratory Armament R&D Center US Army AMCCOM ATTN: Dr. M. A. Hussain Dr. Julian Wu Dr. John Underwood Mr. D. P. Kindall Dr. J. Throup Dr. E. Schneider Watervliet, NY 12189
1	Commander US Army Aviation Research and Development Command ATTN: AMSAV-E 4300 Goodfellow Boulevard St. Louis, MO 63120

DISTRIBUTION LIST

No. of Copies	Organization
1	Director US Army Air Mobility Research and Development Laboratory Ames Research Center Moffett Field, CA 94035
1	Commander US Army Communications Research and Development Command ATTN: AMSEL -ATDD Fort Monmouth, NJ 07703
1	Commander US Army Electronics Research and Development Command Technical Support Activity ATTN: AMDSD -L Fort Monmouth, NJ 07703
1	Commander US Army Harry Diamond Laboratory ATTN: DELHD-TA-L 2800 Powder Mill Road Adelphi, MD 20783
1	Commander US Army Missile Command ATTN: AMSMI-R Redstone Arsenal, AL 35898
1	Commander US Army Missile Command ATTN: AMSMI -YDL Redstone Arsenal, AL 35898
1	Director US Army BMD Advanced Technology Center ATTN: CRDABH-5, W. Loomis P. O. Box 1500, West Station Huntsville, AL 35807
2	Commander US Army Mobility Equipment Research & Development Command ATTN: AMDME -WC AMSME -RZT Fort Belvoir, VA 22060
1	Commander US Army Tank Automotive Command ATTN: AMSTA -TSL Warren, MI 48090
1	Commander US Army Development and Employment Agency ATTN: MODE-TED-SAB Fort Lewis, WA 98433
1	Commander US Army Electronics Proving Ground ATTN: Tech Lib Fort Huachuca, AZ 85613
3	Commander US Army Materials and Mechanics Research Center ATTN: AMXMR -T, J. Mescall AMXMR -T, R. Shea AMXMR -H, S. C. Chou Watertown, MA 02172
5	Commander US Army Research Office ATTN: Dr. R. Weigle Dr. E. Saibel Dr. G. Mayer Dr. F. Smiedeshoff Dr. J. Chandra P. O. Box 12211 Research Triangle Park, NC 27709-2211

DISTRIBUTION LIST

No. of Copies	Organization
2	Commander US Army Research and Standardization Group (Europe) ATTN: Dr. B. Steverding Dr. F. Rothwarf Box 65 FPO NY 09510
1	Director US Army TRADOC Systems Analysis Activity ATTN: ATAA-SL White Sands Missile Range NM 88002
1	Commandant US Army Infantry School ATTN: ATSH-CD-CSO-OR Fort Benning, GA 31905
1	Office of Naval Research Department of the Navy ATTN: Code 402 Washington, DC 20360
3	Commander US Naval Air Systems Command ATTN: AIR 604 Washington, DC 20360
1	Commander Naval Sea Systems Command Washington, DC 20360
3	Commander Naval Surface Weapons Center ATTN: Dr. W. H. Holt Dr. W. Mock Tech Lib Dahlgren, VA 22448
2	Commander Naval Surface Weapons Center ATTN: Dr. J. Frasier Tech Lib Silver Spring, MD 20910

No. of Copies	Organization
1	AF Wright Aeronautical Laboratories AF Systems Command Materials Lab ATTN: Dr. John P. Henderson Wright-Patterson AFB, OH 45433
5	Commander US Naval Research Laboratory ATTN: C. Sanday R. J. Weimer Code 5270, F. MacDonald Code 2020, Tech. Lib Code 7786, J. Baker Washington, DC 20375
4	Air Force Armament Laboratory ATTN: J. Foster John Collins Joe Smith Guy Spitale Eglin AFB, FL 32542
1	RADC (EMTLD, Lib) Griffiss AFB, NY 13441
1	AFWL/SUL Kirtland AFB, NM 87117
1	AUL (3T-AUL-60-118) Maxwell AFB, AL 36112
1	Air Force Wright Aeronautical Laboratories Air Force Systems Command Materials Laboratory ATTN: Dr. Theodore Nicholas Wright-Patterson AFB, OH 45433
1	Director Lawrence Livermore Laboratory ATTN: Dr. M. L. Wilkins P. O. Box 808 Livermore, CA 94550

DISTRIBUTION LIST

No. of Copies	Organization
	Director
6	Sandia National Laboratories ATTN: Dr. L. Davison Dr. P. Chen Dr. L. Bertholf Dr. W. Herrmann Dr. J. Nunziato Dr. S. Passman Albuquerque, NM 87115
1	Director Jet Propulsion Laboratory ATTN: Lib (TDS) 4800 Oak Grove Drive Pasadena, CA 91109
4	SRI International ATTN: Dr. Donald R. Curran Dr. Donald A. Shockey Dr. Lynn Seaman Dr. R. Caligiuri 333 Ravenswood Avenue Menlo Park, CA 94025
1	Aeronautical Research Associates of Princeton Incorporated ATTN: Ray Gogolewski 1800 Old Meadow Rd., #114 McLean, VA 22102
1	Honeywell, Inc. Defense Systems Division ATTN: Dr. Gordon Johnson 600 Second Street, NE Hopkins, MN 55343
2	Orlando Technology, Inc. ATTN: Dr. Daniel Matuska Dr. John J. Osborn P. O. Box 855 Shalimar, FL 32579
1	System Planning Corporation ATTN: Mr. T. Hafer 1500 Wilson Boulevard, Suite 1500 Arlington, VA 22209
3	California Institute of Technology Division of Engineering and Applied Science ATTN: Dr. J. Mikowitz Dr. E. Sternberg Dr. J. Knowles Pasadena, CA 91102
1	Denver Research Institute University of Denver ATTN: Dr. R. Recht P. O. Box 10127 Denver, CO 80210
3	Rensselaer Polytechnic Institute ATTN: Prof. E. H. Lee Prof. E. Krempl Prof. J. Flaherty Troy, NY 12181
1	Southwest Research Institute ATTN: Dr. Charles Anderson 6220 Culebra Road P. O. Drawer 28510 San Antonio, TX 78228
2	Southwest Research Institute Department of Mechanical Sciences ATTN: Dr. U. Kindholm Dr. W. Baker 8500 Culebra Road San Antonio, TX 78228
1	University of Dayton Research Institute ATTN: Dr. S. J. Bless Dayton, OH 45469

DISTRIBUTION LIST

No. of Copies	Organization
1	Brown University Division of Engineering ATTN: Prof. H. Kolsky Providence, RI 02912
3	Carnegie Mellon University Department of Mathematics ATTN: Dr. D. Owen Dr. M. E. Gurtin Dr. B. D. Coleman Pittsburgh, PA 15213
1	Cornell University Department of Theoretical and Applied Mechanic ATTN: Dr. Y. H. Pao Ithaca, NY 14850
1	Forrestal Research Center AeronauticalEngineering Lab. Princeton University ATTN: Dr. A. Eringen Princeton, NJ 08540
1	Harvard University Division of Engineering and Applied Physics ATTN: Prof. J. R. Rice Cambridge, MA 02138
1	Iowa State University Engineering Research Laboratory ATTN: Dr. A. Sedov Ames, IA 50010
1	Pennsylvania State University Engineering Mechanical Dept. ATTN: Prof. N. Davids University Park, PA 16802
1	Rice University ATTN: Dr. R. Bowen P. O. Box 1892 Houston, TX 77001
3	The Johns Hopkins University ATTN: Prof. R. B. Pond, Sr. Prof. R. Green Prof. W. Sharpe 34th and Charles Streets Baltimore, MD 21218
1	Tulane University Dept. of Mechanical Engineering ATTN: Dr. S. Cowin New Orleans, LA 70112
3	University of California ATTN: Dr. M. Carroll Dr. W. Goldsmith Dr. P. Naghdi Berkeley, CA 94720
1	University of California Dept. of Aerospace and Mechanical Engineering Science ATTN: Dr. Y. C. Fung P. O. Box 109 La Jolla, CA 92037
1	University Of California Department of Mechanics ATTN: Dr. R. Stern 504 Hilgard Avenue Los Angeles, CA 90024
1	University of Delaware Dept. of Mechanical Engineering ATTN: Prof. J. Vinson Newark, DE 19711
1	University of Delaware Dept. of Mechanical and Aerospace Engineering ATTN: Dr. Minoru Taya Newark, DE 19711

DISTRIBUTION LIST

No. of Copies	Organization
1	University of Florida Dept. of Engineering Science and Mechanics ATTN: Dr. L. Malvern Gainesville, FL 32601
2	University of Houston Department of Mechanical Engineering ATTN: Dr. T. Wheeler Dr. R. Nachlinger Houston, TX 77004
1	University of Minnesota Dept of Aerospace Engineering and Mechanics ATTN: Prof. J. L. Erickson 107 Akerman Hall Minneapolis, MN 55455
1	University of Washington Dept. of Aeronautics and Astronautics ATTN: Dr. Ian M. Fyfe 206 Guggenheim Hall Seattle, WA 98105
1	Dr. Daniel C. Drucker Graduate Research Professor of Engineering Sciences 231 Aerospace Engineering Bldg. University of Florida Gainesville, FL 32611
1	Washington State University Department of Physics ATTN: Dr. R. Fowles Pullamn, WA 99163
2	Yale University ATTN: Dr. B. T. Chu Dr. E. Onat 400 Temple Street New Haven, CT 06520

Aberdeen Proving Ground

Dir, USAMSAA
ATTN: AMXSY-D
AMXSY-MP, H. Cohen
Cdr, USATECOM
ATTN: AMSTE-TO-F
Cdr, CRDC, AMCCOM
ATTN: SMCCR-RSP-A
SMCCR-MU
SMCCR-SPS-IL

USER EVALUATION SHEET/CHANGE OF ADDRESS

This Laboratory undertakes a continuing effort to improve the quality of the reports it publishes. Your comments/answers to the items/questions below will aid us in our efforts.

1. BRL Report Number _____ Date of Report _____

2. Date Report Received _____

3. Does this report satisfy a need? (Comment on purpose, related project, or other area of interest for which the report will be used.) _____

_____

_____

4. How specifically, is the report being used? (Information source, design data, procedure, source of ideas, etc.) _____

_____

_____

5. Has the information in this report led to any quantitative savings as far as man-hours or dollars saved, operating costs avoided or efficiencies achieved, etc? If so, please elaborate. _____

_____

_____

6. General Comments. What do you think should be changed to improve future reports? (Indicate changes to organization, technical content, format, etc.)

_____

_____

_____

CURRENT ADDRESS

_____
Name

_____
Organization

_____
Address

_____
City, State, Zip

7. If indicating a Change of Address or Address Correction, please provide the New or Correct Address in Block 6 above and the Old or Incorrect address below.

OLD ADDRESS

_____
Name

_____
Organization

_____
Address

_____
City, State, Zip

(Remove this sheet along the perforation, fold as indicated, staple or tape closed, and mail.)

FOLD HERE

Director
US Army Ballistic Research Laboratory
ATTN: AMXBR-OD-ST
Aberdeen Proving Ground, MD 21005-5066

NO POSTAGE
NECESSARY
IF MAILED
IN THE
UNITED STATES

OFFICIAL BUSINESS
PENALTY FOR PRIVATE USE, $300

BUSINESS REPLY MAIL
FIRST CLASS PERMIT NO 12062 WASHINGTON, DC
POSTAGE WILL BE PAID BY DEPARTMENT OF THE ARMY

Director
US Army Ballistic Research Laboratory
ATTN: AMXBR-OD-ST
Aberdeen Proving Ground, MD 21005-9989

FOLD HERE

END

FILMED

3-85

DTIC